

Global patterns of tectonic stress

Mary Lou Zoback, Mark D. Zoback, J. Adams, M. Assumpção, S. Bell, E. A. Bergman, P. Blümling, N. R. Brereton, D. Denham, J. Ding, K. Fuchs, N. Gay, S. Gregersen, H. K. Gupta, A. Gvishiani, K. Jacob, R. Klein, P. Knoll, M. Magee, J. L. Mercier, B. C. Müller, C. Paquin, K. Rajendran, O. Stephansson, G. Suarez, M. Suter, A. Udias, Z. H. Xu & M. Zhizhin

Regional patterns of present-day tectonic stress can be used to evaluate the forces acting on the lithosphere and to investigate intraplate seismicity. Most intraplate regions are characterized by a compressional stress regime; extension is limited almost entirely to thermally uplifted regions. In several plates the maximum horizontal stress is subparallel to the direction of absolute plate motion, suggesting that the forces driving the plates also dominate the stress distribution in the plate interior.

TWO primary categories of forces are responsible for the state of stress in the upper, elastic part (reaching to depths of 10–35 km) of the Earth's lithosphere. The first category is responsible for what we shall call here 'tectonic stresses'. These broad-scale forces include plate-boundary forces (which either drive or resist plate motion), forces resulting from geodynamic processes (including broad-scale flexure of the lithosphere owing to surface and subsurface loads and/or inhomogeneous density distributions), and thermoelastic forces in cooling oceanic lithosphere. The second category is derived from local effects of topography, anisotropy of strength or elastic properties, and effects of erosion and man-made excavation; these forces generate local or 'induced' stresses. Spatial uniformity of the *in situ* stress field generally allows us to distinguish easily between these two categories. For example, tectonic stresses typically are uniform over distances many times (from 2–3 times to more than 100 times) the thickness of the elastic part of the lithosphere, whereas local stresses have wavelengths that are a fraction of this thickness. Induced stresses are critical in many mining and civil-engineering situations, but tectonic stresses provide valuable constraints on a variety of broad-scale geological problems such as the relative magnitudes of plate-driving forces and the nature of deformation and seismicity in the plate interior, far from plate boundaries (so-called intraplate or midplate deformation).

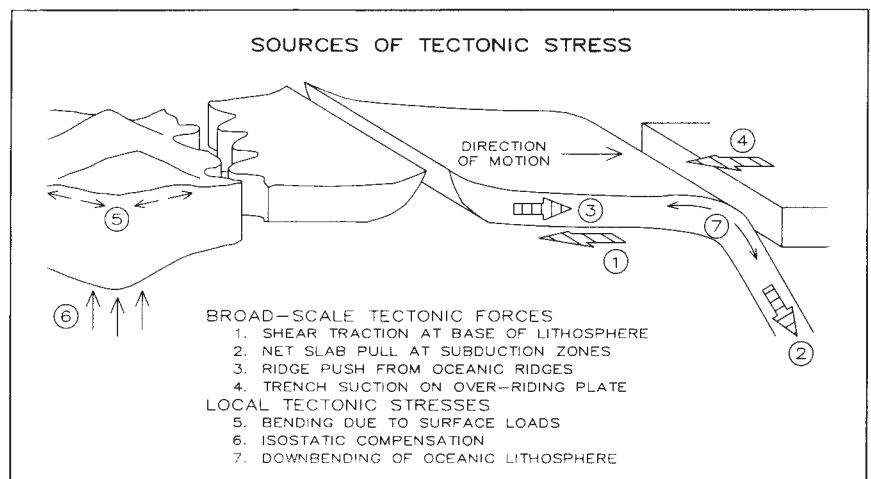
The World Stress Map project of the International Lithosphere Program is compiling a global database of contemporary *in situ* stresses in the crust using a variety of geophysical and geological measurement techniques. The project is a collaborative effort which at present involves over 30 scientists from 19 different countries. This project builds on early investigations of stress patterns in central and eastern North America and in western Europe, which indicated that both horizontal stress orientations and relative stress magnitudes are uniform over broad regions of the Earth's crust^{1–10}. A comprehensive compilation and analysis of the state of stress of the contiguous United States¹¹ which used both geological and geophysical stress indicators, confirmed the regionally uniform stress orientations found in the earlier studies and also concluded that stress orientations inferred from different types of indicator were generally consistent, despite the variety of techniques being used and the different ranges of depth being sampled.

Here we focus on these regionally uniform, broad-scale stress fields in the lithosphere. The most probable sources of such stress fields are

the major forces acting on lithospheric plate boundaries. These forces include: shear tractions at the base of the lithosphere that can either drive or resist plate motion; a 'slab pull' force which represents a balance between the negative buoyancy of the subducted oceanic lithosphere, viscous drag on the subducting slab and frictional resistance to subduction at shallow depth; resistance to continent–continent collision; a 'ridge push' force resulting from the excess thermal elevation of young oceanic lithosphere; and a 'trench suction' force exerted on the overriding plate at subduction zones, which is caused by trenchward extension of this plate to fill the gap that results from the falling back of the subducted slab (see refs 12–19 for detailed discussions of these forces).

Geological evidence, thermodynamic considerations¹⁷ and relatively short timescales for changes in plate motion all suggest that viscous drag at the base of the plates resists, rather than drives, plate motion and probably balances the torque caused by driving forces on individual plates^{19,20}. Drag forces thus tend to act antiparallel to the direction of 'absolute' plate motion relative to the lower mantle. Slab-pull, trench-suction and collisional-resistance forces all act normal to plate boundaries. The ridge-push force is an integrated force acting over the cooling oceanic lithosphere and generally acts normal to the plate boundary, except where spreading is oblique to the ridge. Here we shall approximate the orientation of the ridge-push force within a plate by the local orientation of relative motion calculated from the pole of opening for mid-ocean-ridge segments.

More localized sources of tectonic stress include flexural (bending) stresses caused by surface loads supported by the strength of the lithosphere (for example, resulting from sediment



deposition or volcanic loading, mountain building and erosion), by subsurface loads required for isostatic compensation of topography (that is, adjustment of lithospheric density in response to variability of overlying load), by down-bending of the oceanic lithosphere in subduction zones, and by membrane stresses generated by the motion of plates over an Earth of varying radius of curvature²¹. From a global perspective perhaps the most significant of these forces is the combined effect of the surface load and the buoyancy of a low-density region (thickened crust and/or thin mantle lithosphere) supporting a region of high topography. If the buoyancy forces dominate they can produce a broad zone of deviatoric tension beneath major mountain ranges and high plateaus^{18,22,23}.

As indicated previously, lateral variations in strength or elastic properties can result in local induced stresses. However, in some cases these variations are so profound and are of such long wavelength that they dominate the tectonic stress field. The best documented example of this effect is an apparent ~50–60° rotation of the horizontal stresses in a 100–125-km-wide zone on either side of the right-lateral San Andreas fault in California, the boundary between the Pacific and North American plates. It is suggested that this rotation results from an extremely low shear strength of the San Andreas fault and the slightly convergent relative motion between the two plates^{24,25}. Geological and focal-mechanism data²⁶ suggest that a similar stress rotation occurs adjacent to the right-lateral strike-slip Alpine fault in New Zealand, the plate boundary between the Pacific and Indian-Australian plates.

Stress measurement

A variety of data indicate that the three principal stresses in the Earth's upper crust lie in approximately horizontal and vertical planes¹¹, as suggested by E. M. Anderson²⁷. Thus, the orientation of the principal axes of the stress tensor can be constrained by specifying the azimuth of one of the horizontal principal stresses. Absolute stress magnitudes at depths of earthquake generation are extremely difficult to obtain and it is generally possible to constrain relative stress magnitudes only from the style of active faulting or deformation occurring in a region (see box).

- *In situ* stresses in the elastic part of the Earth's lithosphere are compressive (below the upper tens of metres).
- Principal stresses lie in approximately horizontal and vertical planes:
 - S_v = vertical stress $\approx \rho gz$
 - S_{Hmax} = maximum horizontal stress
 - S_{Hmin} = minimum horizontal stress
- Relative stress magnitudes determine type of deformation:
 - Normal faulting: $S_v > S_{Hmax} > S_{Hmin}$
 - Strike-slip faulting: $S_{Hmax} > S_v > S_{Hmin}$
 - Thrust or reverse faulting: $S_{Hmax} > S_{Hmin} > S_v$

Four different categories of geophysical and geological data are used at present as reliable indicators of horizontal stress orientations: earthquake focal mechanisms, stress-induced well-bore enlargements or 'breakouts', *in situ* stress measurements, including hydraulic fracturing and stress-relief measurements, and young geological deformational features, including both fault-slip and volcanic alignments.

A quality ranking system was developed recently²⁸ to aid in the analysis of the tectonic stress field in the lithosphere. This system permits a comparison of data collected by these different techniques and, in particular, aids in evaluating the significance of data in areas of sparse coverage. The ranking criteria are based both on the accuracy of individual determinations and on the relative reliability of the technique as an indicator of tectonic (as opposed to local or induced) stress. Four qualities are used, ranked in the order $A > B > C > D$. An A quality is assigned to data that record the tectonic stress field to within ± 10 – 15° , a B quality to within ± 15 – 20° , and a C quality to within $\pm 25^\circ$. In some cases D-quality data may record the *in situ* stress field reasonably accurately but because of a variety of potential perturbing factors (such as topography and free-surface effects) these data are not generally considered to be reliable indicators of tectonic stress.

These four main types of stress indicator have been described previously^{2,11,19,28}. The major recent advances that have made possible the compilation of global stress data are as follows.

Borehole breakouts as a reliable indicator of horizontal tectonic stress orientation. According to elastic theory, the maximum compressive circumferential stress developed around a vertical borehole is centred on the azimuth of the least horizontal far-field stress (S_{Hmin}), and the minimum stress occurs in the direction of the maximum horizontal stress (S_{Hmax})²⁹ (Fig. 1). Well-bore breakouts are a natural phenomenon that result from shear fracturing in the region of maximum stress amplification^{30,31}; they cause a cross-sectional enlargement of the hole in the direction of S_{Hmin} . In contrast, hydraulic fracturing is an active technique in which a portion of the well-bore is isolated and pressurized by injected fluids until a tensile fracture develops in the direction of S_{Hmax} . The orthogonality of breakouts and hydraulic fractures within a single well has now been confirmed by down-hole experiments in several wells in various tectonic settings^{31–33}.

Numerous investigations have established that consistently oriented breakouts form within an individual well and in wells within a given field^{32–39}. This possibility of multiple determinations in an individual well, and the ability to check for regional consistency among numerous wells, make breakout data valuable indicators of stress orientation. In addition, because wells for petroleum exploration and production are often drilled to depths of 3–4 km (and in some areas, up to 5–6 km), breakout data help to bridge the gap between the near-surface stress indicators (which sample typically less than 1 km depth) and

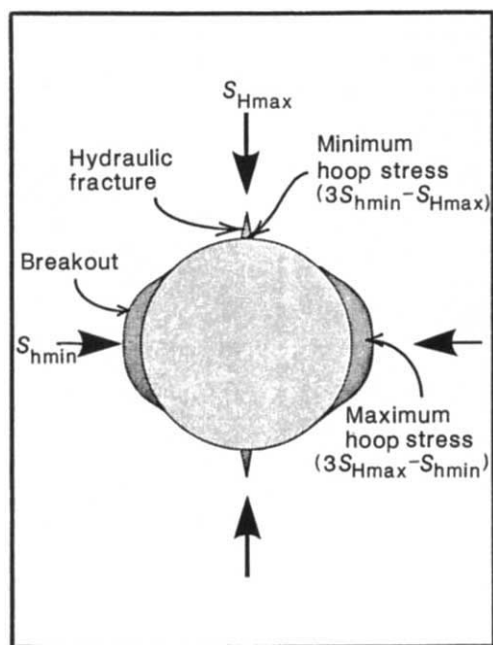


FIG. 1 Stress concentration around a vertical circular hole in an elastic half-space subjected to unequal far-field horizontal stresses, S_{Hmax} and S_{Hmin} . As indicated, breakouts and hydraulic fractures form as a result of these stress concentrations.

earthquake focal mechanisms (of typically 5–15 km depths). As can be seen in Fig. 2, there is generally an excellent agreement locally between stress orientations determined from well-bore breakouts and those inferred from earthquake focal mechanisms^{25,28}.

Resolution of earthquake focal mechanisms. Largely as a result of waveform modelling made possible by digital seismic acquisition networks, more and better-constrained focal mechanisms are now available. In addition, routine moment-tensor inversion of global network events⁴⁰ has greatly increased the database. An inherent difficulty remains, however, in estimating principal stress directions from focal mechanisms^{41–43}. Focal mechanisms are constructed from the radiation pattern of seismic waves, which defines a set of two possible orthogonal fault planes and slip vectors. P and T axes correspond to the maximum shortening and extensional strain directions for these shear faults.

But most crustal earthquakes are presumed to occur on pre-existing faults, in which case the fault-slip vector is a function of the orientation of the pre-existing fault and of both the orientations of the principal stresses and their relative magnitudes^{41,44–46}. Because of the uncertainty in inferring stress directions from earthquake focal mechanisms, a single mechanism, regardless of how well constrained, does not receive an A-quality ranking. This highest ranking is reserved for stress directions determined from mean P- or T-axis orientations or formal inversions for best-fitting stress axes^{47–51} of groups of moderate-sized earthquakes (at least one event with magnitude >4.5) occurring within close geographical proximity and with a variety of focal mechanisms. When using average P and T axes it is commonly assumed that errors resulting from slip on pre-existing planes of a variety of trends tend to cancel statistically^{11,52}. In general, aftershock sequences are not used because in some cases they appear to record deformation that is a secondary adjustment in response to slip in the main shock^{53,54}. A number of cases, however, show no discernible differences in stress orientation and relative magnitudes before and after the main shock^{55,56}.

Inversion algorithms to infer deviatoric stress tensors from fault slip and focal mechanism data^{46–51,57–59}. The underlying assumption of these inversion algorithms is that the measured slip vectors represent the direction of maximum resolved shear stress on the fault planes^{44,45}. Slip vectors, determined from striations observed on small fault planes of a variety of attitudes along active fault zones, are then inverted to yield a best-fitting deviatoric stress tensor. The inversion methods for fault-slip data^{48,57–59} are essentially the same as those used for focal-mechanism data^{47,49–51} and, in both cases, yield principal stress orientations that are generally well constrained⁵⁰. However, fault-slip inversions yield more precise information on relative stress magnitudes, because the true fault plane is known. The validity of this technique has been established by numerous studies which have demonstrated a reasonable match between predicted and observed slip vectors⁴⁸.

Often, particularly for historical earthquakes, only the overall slip vector and general attitude of the fault plane are known. In this case the data are treated as a palaeo-focal mechanism and the stress directions are inferred by the method of Raleigh⁴². These data are generally given a B-quality ranking. C-quality fault-slip stress determinations are estimated from the general attitude and primary sense of offset (but not actual slip vector) on an active fault plane.

Volcanic alignments as reliable horizontal stress indicators⁶⁰. Volcanic feeder vents such as dykes and cinder cones propagate perpendicular to the minimum principal far-field stress as natural, large-scale hydraulic fracturing experiments⁶¹. Thus, the mean strike of vertical dykes corresponds to the direction of S_{Hmax} . To study the current state of stress one uses vents of Quaternary age; however, palaeo-stress can be similarly studied using older dykes or cinder cones that are radiometrically dated.

Critical evaluation of stress relief measurements. One of the earliest and best studied techniques for investigating the state of stress in the Earth's crust is stress-relief measurements, commonly referred to as 'overcoring' measurements. This technique involves determination of the natural three-dimensional deformation (strain) relieved in a body rock *in situ* when separated from the surrounding rock volume^{62,63} and is the only technique that measures the complete stress tensor. Amongst the primary drawbacks of this method are that the measurements must be made near a free surface (either the Earth's surface or an excavated surface in a mine), that the strain relief is determined over areas of only a few mm² to cm², and that the change of stress on overcoring must be calculated from the strain relief, which requires knowledge of the complete compliance tensor. In particular, near-surface surface-stress-relief measurements have been shown to be subject to effects of local topography, rock anisotropy and natural fractures⁶⁴. Because of these difficulties, we have assigned a D quality to all near-surface (<5–10 m, depending on local site conditions) stress-relief measurements in the database. For stress-relief measurements made at depths >10 m (or at least one excavation diameter away from the free surface in a mine) the assigned data quality depends on the internal consistency of multiple measurements.

Global stress patterns

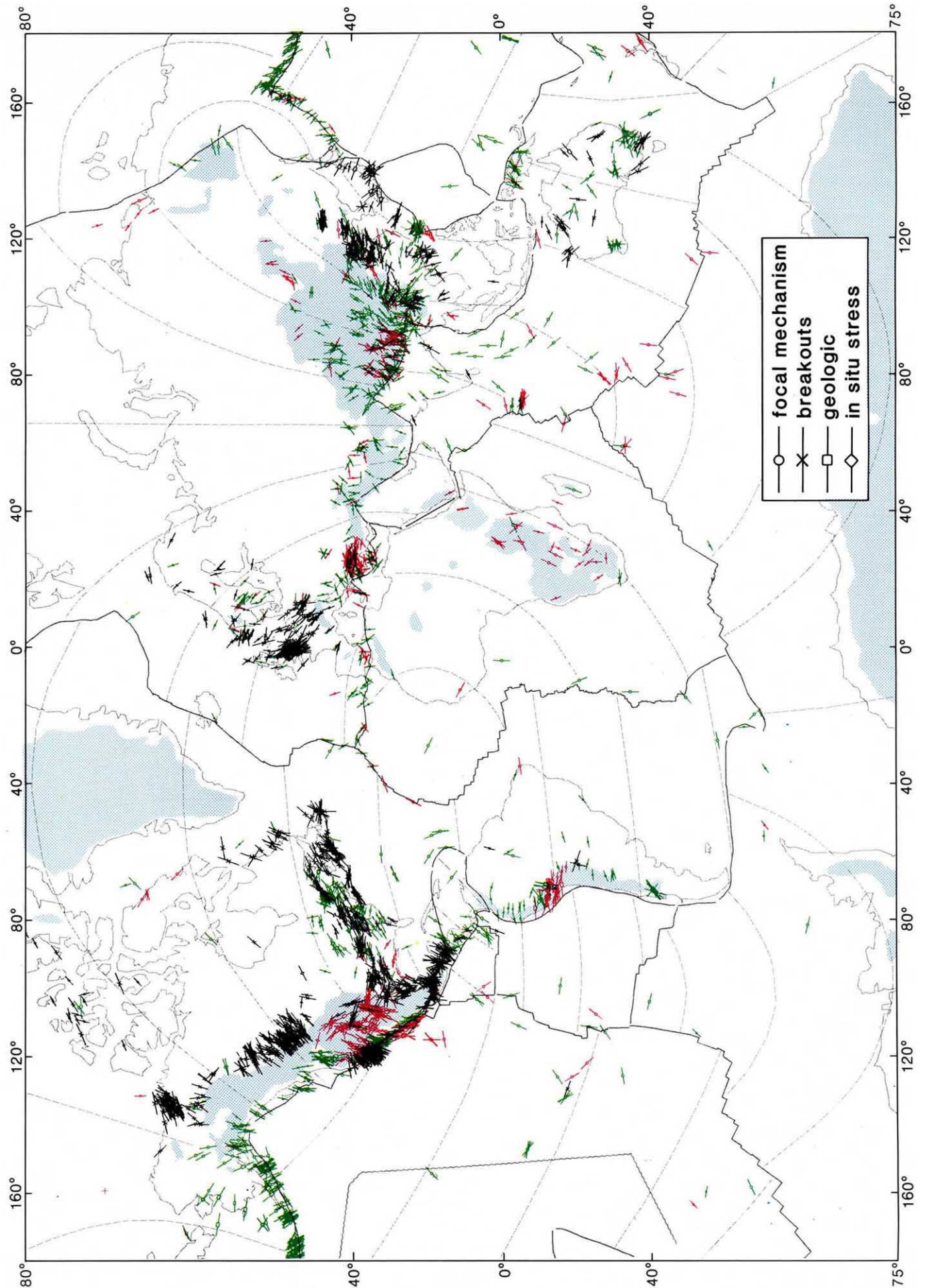
The first global map of stress orientations was published by Ranalli and Chandler in 1975⁶⁴ and contained 59 stress-relief measurements. In 1979, Richardson *et al.*¹⁹ presented a map containing about 133 points worldwide, derived primarily from earthquake focal mechanisms supplemented by surface overcoring measurements and geological data. Much of the data shown on these maps we would now categorize as rather low-quality (C or D) indicators of tectonic stress.

At present there are 3,574 entries in our global database; 3,142 of them are assigned either an A, B or C quality and are plotted on Fig. 2. As mentioned earlier, the emphasis in this paper is on the tectonic stress field, so D-quality data are not plotted. The length of each data point in Fig. 2 is proportional to its quality and the centre symbol designates the type of stress indicator. The distribution of the data by measurement type is as follows: earthquake focal mechanisms, 50%; breakouts, 31%; hydraulic fracturing measurements, 3%; stress relief, 7%; volcanic alignments, 4%; and fault-slip data, 5%. Distribution of areal coverage according to quality is given in Table 1.

A single horizontal stress orientation, S_{Hmax} , is plotted on Fig. 2 to facilitate the recognition of regional patterns of stress orientation. Relative stress magnitudes (stress regime) are indicated by colour for all data for which they are directly determined. Plotted in red are data that indicate an extensional stress regime (defined here as one in which the vertical stress is the

TABLE 1 Areal distribution of data

Area	A quality	B quality	C quality
N. American plate	450	635	555
USA	189	398	402
Canada	160	158	101
Mexico	93	69	28
Central America	8	10	24
S. American plate	7	5	23
Eurasian plate	100	388	577
Europe	66	83	181
Asia	34	305	396
Indo-Australia plate	16	74	99
Pacific plate	0	28	2
Africa plate	0	22	37
Antarctica plate	0	22	7
Nazca plate	0	9	0
Cocos plate	0	4	0



◀ FIG. 2 World stress map, transverse mercator projection. S_{Hmax} orientations are plotted, length of lines are proportional to quality (A, B or C). Because the data coverage is so dense in the western United States, only A- and B-quality data are plotted there. Centre symbol designates type of stress indicator. Data indicating an extensional stress regime are plotted in red, data for a compressional regime are plotted in green, and data where stress regime is unknown are plotted in black. All regions with average elevation greater than 1 km are indicated by blue shading. Lightly dashed lines correspond to absolute velocity trajectories determined using AM1–2 poles of Minster and Jordan⁶⁵. Wavy line approximates the 80-Myr isochron on the Pacific plate.

greatest principal stress); normal or combined normal and strike-slip faulting characterize this regime. The data in green indicate a compressional stress regime, in which one or both of the horizontal stresses are greater than the vertical stress; deformation in this regime is characterized by thrust, strike-slip or combined thrust and strike-slip faulting. Stress orientations for which information on relative stress magnitudes was not determined directly or not reported are plotted in black. Unfortunately this is the case for all of the breakout data, which comprise nearly one-third of the data set.

Regions with average elevation greater than 1,000 m are indicated on Fig. 2 by shading. Also shown are absolute plate-velocity trajectories, calculated using Minster and Jordan's⁶⁵ poles of angular motion for each plate (model AM1–2).

Three broad generalizations can be drawn from the data. (1) Most midplate regions are characterized by compressive stress regimes, that is, by thrust and/or a combination of thrust and strike-slip deformation. (2) Most continental areas of extensional stress regimes (normal or combined normal and strike-slip faulting) are regions of anomalously high elevation (for example, the western US Cordillera, the East African rift, the Baikal rift, the Himalayas and the Andes). (3) Broad regions of the Earth's crust are subjected to a nearly uniformly oriented stress field, specifically a $\sim 2 \times 10^7$ -km² region (approximately one-eighth of the world's land surface) of north-east to east-north-east compression in central and eastern North America and a $\sim 6 \times 10^6$ -km² region of north-west to north-north-west compression in western Europe.

In the midplate portions of some plates there is a striking correlation between S_{Hmax} orientations and azimuths of absolute plate velocity (as indicated by the trajectories in Fig. 2). This correlation is illustrated by the histograms in Fig. 3, which show, point by point, the angular difference between the observed S_{Hmax} orientation and the local absolute-velocity azimuth. In these plots the local absolute-plate-velocity direction is the reference direction; hence positive angles in Fig. 3 represent observed S_{Hmax} directions oriented clockwise with respect to that reference direction. It is important to note that because these histograms represent a point-by-point count and not a regionally averaged fit, they are strongly influenced by regions of dense data distribution. Furthermore, all data of A to C quality are treated equally, not weighted by quality.

Figure 3 indicates a strong positive correlation between S_{Hmax} orientations and absolute velocity directions on the two fastest-moving continental plates: midplate North America (including most of the central and the eastern United States, much of Canada and possibly the western Atlantic basin) and the South American plate. The correlation is particularly striking for midplate North America, the area of densest and highest-quality data coverage in the world; here the angular differences show a near-normal distribution about the reference absolute velocity direction. Breakouts on the outer continental shelf in eastern North America contribute to scatter in the histogram (see shaded areas on Fig. 3); detailed analysis of these data indicate that S_{Hmax} orientations are often rotated into a plane approximately parallel to the local trend of the continental slope. This rotation may be the result of superposition of stresses owing to flexure from sediment loading on the continental shelf⁶⁶.

The strong positive correlation between S_{Hmax} and absolute velocity directions for midplate North America has been interpreted by some workers as indicating that resistive drag at the base of the plate is the primary source of stress in the upper lithosphere⁶⁷. However, as pointed out previously, the absolute velocity vector in midplate North America coincides within $\sim 10^\circ$ with the expected direction of the ridge-push force from the Mid-Atlantic Ridge^{28,68–70}; therefore the two mechanisms cannot be distinguished as possible sources of stress for this plate. Similarly, for the South American plate, the approximately east-west absolute velocity is within 10° of the ridge-push direction inferred from the South American–African pole of relative motion. In addition, convergence between the South American plate and both the Nazca and Pacific plates is also approximately east-west. Thus, for both the North and South American plates it is not apparent which source of stress, if any, is dominant. Overall, the simplest explanation for the correlation between S_{Hmax} and absolute-plate-velocity directions on these plates is that the net balance of forces that move the plates dominates the stress distribution within the plate interiors.

In western Europe the S_{Hmax} directions and absolute-plate-velocity directions seem to be relatively well correlated (Fig. 2), except in the Aegean. However, as indicated in Fig. 3, the data consistently indicate a clockwise rotation of S_{Hmax} with respect to the absolute-velocity direction, that is, the observed S_{Hmax} orientations trend more northerly than the west-north-west absolute-velocity field. S_{Hmin} directions in the Aegean region (orthogonal to the S_{Hmax} directions shown in Fig. 3) are also clockwise with respect to the direction of plate motion. However, it should be noted that the absolute-velocity rotation pole for Eurasia is very poorly constrained because this plate is moving so slowly in an absolute reference frame⁶⁵. Thus, the significance of the difference between the S_{Hmax} and absolute-velocity direction is unclear.

Another potentially significant source of stress in Western Europe is the force resulting from the continental convergence of the African and Eurasian plates. Overall, S_{Hmax} orientations seem to be relatively well correlated with the predicted convergence velocity field obtained using the African–Eurasian pole of relative motion from the NUVEL velocity model⁷² (see histogram in the lowermost left corner of Fig. 3). S_{Hmax} orientations in the Aegean are generally orthogonal to the convergence direction (see below). However, the average S_{Hmax} direction of N 42° W obtained from the extensive breakout data set in the United Kingdom⁷¹ is more northerly than that predicted from the velocity field for this region on the basis of either the absolute-velocity directions (N 62° W), ridge-push forces (N 70° W), or continental-convergence forces (N 56° W). To properly evaluate the stress field resulting from these plate-boundary forces, however, detailed two- or three-dimensional finite-element modelling is needed.

There is the suggestion of a weak correlation between S_{Hmax} and absolute-velocity directions in the Pacific plate, although the data for this plate are few in number and derived primarily from earthquake focal mechanisms. Data from older (north-western and western) portions of the Pacific plate have S_{Hmax} orientations that are generally orthogonal to absolute-velocity directions (Fig. 3). S_{Hmax} orientations in the younger portions of the Pacific plate are quite scattered with respect to absolute plate motion; however, if events near the East Pacific Rise are excluded, S_{Hmax} orientations in the younger portions of the plate are sub-parallel to the absolute plate-velocity direction (Fig. 2). Interestingly, this change in S_{Hmax} orientations coincides roughly with the 80-Myr isochron, the point at which the $t^{1/2}$ subsidence of cooling oceanic lithosphere dramatically slows down from $t^{1/2}$ to an approximately exponential decay⁷³. However, once again, spreading directions in the Pacific Plate, using relative motion poles with respect to both the Nazca and Antarctic plates, are aligned within 10° with absolute plate-motion vectors, so forces owing to ridge push and drag cannot

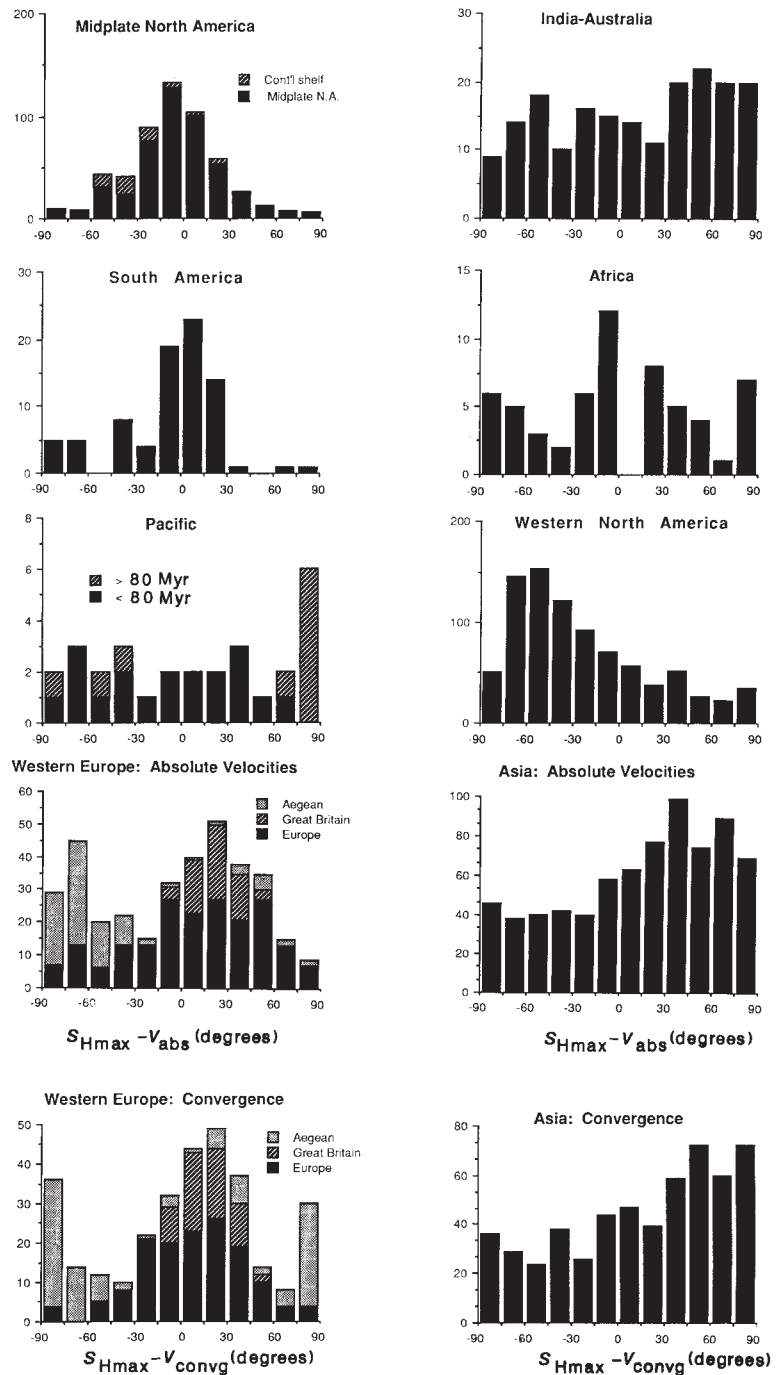


FIG. 3 Histograms comparing, point by point, the angular difference between observed S_{Hmax} orientations and a computed velocity field for specific plates, subplates or regions. Upper four histograms in both columns compare observed stress directions with absolute-velocity directions, and the lowest histogram in each column compares observed stress directions with relative (convergent) velocity directions (see text).

be distinguished. Although single-force finite-element models of resistive drag¹⁹ predict variations in relative stress magnitudes across the Pacific plate that are consistent with the observed stress rotation, it is impossible to determine the source of this apparent polarity change between S_{Hmax} and S_{hmin} without detailed modelling that includes all potential forces acting on the plate.

Figure 2 and the plots in Fig. 3 indicate that there is no clear correlation between S_{Hmax} and absolute velocity in several major regions, for example, much of Asia, the Indian-Australian plate, the African plate and the largely extensional and thermally uplifted western US Cordillera. Data for the Antarctic, Nazca and Cocos plates are too sparse either to confirm or to contradict any possible correlation.

The pattern of stress throughout eastern Asia is strongly influenced by the collision of the Eurasian and Indian-Australian plates. Within the Himalayan collision zone the S_{Hmax} orientations are generally north-south, subparallel to both the absolute motion of the Eurasian plate⁶⁵ and to the relative (convergent) motion between the Eurasian and Indian-Australian plates⁷². However, in eastern China, S_{Hmax} trajectories form a quasi-radial pattern which is oblique to both the absolute and the relative plate-motion directions (see histograms in the lower right corner of Fig. 3). This quasi-radial pattern of S_{Hmax} orientations is well predicted by indenter-type models⁷⁴ for the continued collision of the Eurasian and the Indian-Australian plates.

As indicated on Fig. 2, the pattern of S_{Hmax} orientations for

the Indian–Australian plate is rather complex; in particular, data for the Australian continent, a relatively stable intraplate region, show great variability (in contrast to stress patterns in midplate North America, for example). A high level of intraplate seismicity within the Indian Ocean has attracted a lot of interest in attempts to model the plate-driving and other tectonic forces acting on this plate^{75–77}. In these models, Himalayan collision generally accounts for the north-easterly compression in the eastern Indian Ocean, whereas complex intraplate stress patterns throughout the rest of the plate generally result from the complicated plate geometry and the varying nature of subduction along the Sunda and Tonga–Kermadec arcs.

Regions of extensional stress

As shown in Fig. 2, areas of extension on the continents occur primarily in regions of anomalously high elevation. These areas of extension occur in a variety of tectonic settings: a broad zone of distributed shear (western North America), an intraplate setting (Baikal and African rifts), a continental-collision zone (Himalayas), and above a subduction zone (Andes). The latter two examples are regions of relatively rapid plate convergence in which the extension direction is generally orthogonal to the convergence direction. In contrast, in true ‘back-arc spreading’, extension occurs in a direction generally orthogonal to the arc boundary, so that extension is often subparallel to convergence direction. Modern examples of back-arc spreading generally occur in topographically depressed areas such as the Mariannas basin and other western Pacific basins (all of which are currently unsampled by the database). The modern low elevation of the Aegean region is best explained by Pliocene back-arc spreading which was subsequently replaced by modern (late Pleistocene to present) extension parallel to (that is, S_{Hmax} perpendicular to) the convergence direction⁷⁸ (see histogram in lower left corner of Fig. 3).

The relationship between elevation and extension is complex. For example, a recent analysis⁷⁹ indicates that extension in the high Tibetan Plateau cannot be explained by crustal thickening and elevated topography alone. For this extension to occur concomitant with continued collision and convergence, an additional force must be added to the system, such as a buoyancy force derived from a ‘deblobbing’ or delamination of thickened dense mantle lithosphere.

The contrast in stress patterns between the regionally high western US Cordillera and the ‘midplate’ region of North America suggests that the effects of Pacific–North American plate interaction are not transmitted through the western United States. The source of much of the uplift in the western United States must be thermal (or equivalently, thinned mantle lithosphere), as crustal thickness in much of this region is comparable to or less than that in the eastern United States⁸⁰. Details of the western United States stress pattern have been discussed elsewhere^{24,25,28,81}; however, it is of interest that throughout much of this elevated region the stress regime is extensional. In some cases, abrupt 90° changes in extension direction occur which appear to correlate with lateral changes in lithosphere thickness^{11,28} and thermal regime⁸².

Focal mechanisms within the African plate⁸³ show dominantly normal faulting within the thermally elevated East African rift system; events outside the rift have both strike-slip and normal faulting mechanisms. In southern Africa, overcoring measurements made in deep mines (up to 3 km depth)⁶³ and focal mechanisms suggest a distinct stress regime with a ~90° rotation of S_{Hmax} relative to the East African rift (Fig. 2). The general extensional stress state throughout much of the African plate is inconsistent with a compressional midplate stress field predicted solely from the plate-boundary forces (ridge push from ridges on three sides of the plate and a continental collision along the northern boundary)¹⁹. Furthermore, drag forces on this plate are probably minimal because Africa is moving so slowly in an absolute reference frame⁶⁵. The profound intraplate extension

Authors' affiliations

Mary Lou Zoback¹, Mark D. Zoback², J. Adams³, M. Assumpção⁴, S. Bell⁵, E. A. Bergman⁶, P. Blümling⁷, N. R. Brereton⁸, D. Denham⁹, J. Ding¹⁰, K. Fuchs¹¹, N. Gay¹², S. Gregersen¹³, H. K. Gupta¹⁴, A. Gvishiani¹⁵, K. Jacob¹⁶, R. Klein¹⁷, P. Knoll¹⁸, M. Magee¹, J. L. Mercier¹⁹, B. C. Müller¹¹, C. Paquin²⁰, K. Rajendran²¹, O. Stephansson²², G. Suarez²³, M. Suter²⁴, A. Udias²⁵, Z. H. Xu²⁶ & M. Zhizhin¹⁵.

¹ US Geological Survey, Menlo Park, California 94025, USA; ² Department of Geophysics, Stanford University, Stanford, California 94305, USA; ³ Geophysics Division, Geological Survey of Canada, 1 Observatory Crescent, Ottawa, Ontario, Canada K1A 0Y3; ⁴ Instituto Astronômico e Geofísico, Universidade de São Paulo, 01051 São Paulo-SP, Brazil; ⁵ Institute of Sedimentary and Petroleum Geology, 3303 33rd St NW, Calgary, Alberta, Canada T2L 2A7; ⁶ Massachusetts Institute of Technology, Cambridge, Massachusetts 02139, USA; ⁷ NAGRA, Parkstrasse 23, CH-5401 Baden, Switzerland; ⁸ British Geological Survey, Keyworth, Nottinghamshire NG12 5GG, UK; ⁹ Australian Seismological Centre, PO Box 378, Canberra, ACT 2601, Australia; ¹⁰ Institute of Crustal Dynamics, State Seismological Bureau, PO Box 2855, Beijing, China; ¹¹ Universität Karlsruhe, Geophysikalisches Institut, D-7500 Karlsruhe 21, FRG; ¹² Rock Mechanics Laboratory, Auckland Park 2006, Johannesburg, South Africa; ¹³ Geodetic Institute, Gamlehave Alle 22, DK-2920 Charlottenlund, Denmark; ¹⁴ Cochin University of Science and Technology, Cochin 682 022, India; ¹⁵ Institute of Physics of the Earth, Academy of Sciences of the USSR, Moscow 123810, USSR; ¹⁶ Lamont–Doherty Geological Observatory, Columbia University, Palisades, New York 10964, USA; ¹⁷ BP Research International, Sunbury on Thames, Middlesex TW16 7LN, UK; ¹⁸ Zentralinstitut für Physik der Erde, Telegrafenberg A 17, Potsdam, GDR-1561; ¹⁹ Laboratoire de Géologie Dynamique Interne, Université Paris-Sud, 91405 Orsay, France; ²⁰ Laboratoire de Géophysique et Géodynamique Interne, Université Paris-Sud, 91405 Orsay, France; ²¹ Department of Geology, University of South Carolina, Columbia, South Carolina 29208, USA; ²² Lulea University of Technology, Division of Rock Mechanics, 95187 Lulea, Sweden; ²³ Instituto de Geofísica, Universidad Nacional Autónoma de México, México DF 04510, Mexico; ²⁴ Instituto de Geología, Universidad Nacional Autónoma de México, México DF 04510, Mexico; ²⁵ Cátedra de Geofísica-Fac. de C. Físicas, Universidad Complutense, Madrid 28040, Spain; ²⁶ Institute of Geophysics, State Seismological Bureau, Beijing, China.

in East Africa suggests an additional source of stress, probably related to buoyancy associated with mantle upwelling and lithospheric thinning.

Conclusions and future work

The data and brief interpretations presented here represent a progress report intended to stimulate further interest and participation in the World Stress Map project. Analysis of the data compiled to date, together with the results of a large number of earlier regional studies, permit the following generalizations and conclusions:

- The various stress measurement and analysis techniques used in this study seem to sample contemporary regional stress orientations and show an excellent agreement despite the wide range of depths sampled.
- The state of stress throughout the upper, brittle crust is regionally consistent. This allows the definition of provinces of relatively constant orientations and relative magnitude of stress.
- Most intraplate or midplate regions are characterized by a compressional stress regime, that is, thrust or strike-slip faulting. Extensional stress regimes occur almost exclusively in anomalously high, and often thermally elevated regions, implying superposition of a buoyancy force fundamentally linked to the source of the elevation.
- A strong positive correlation between absolute plate velocity and S_{Hmax} direction for broad regions of several plates implies that the net plate-boundary forces responsible for moving these plates dominate the stress distribution in the plate interior. Evaluation of the relative importance of drag at the base of the plates will require detailed modelling constrained by data on absolute stress magnitudes.
- Local crustal structure, rheology and strength contrasts can strongly influence tectonic-stress orientations. Examples include stress rotation within a ~250-km-wide zone straddling the San Andreas fault and along continental margins.

We have several clear objectives for the future. First, we are currently cooperating with industry to obtain additional well-bore breakout data to fill in many of the gaps in the map; targeted areas include South America, Africa, the Middle East and south-east Asia. The oceans, which cover 70–75% of the Earth's surface, are greatly undersampled. Breakout analyses in two Deep Sea Drilling Project holes⁸⁴ confirmed the mean S_{Hmax} orientation inferred from nearby focal mechanisms, and established the feasibility of this stress-measurement technique in future Ocean Drilling Program holes. The oceanic data are essential for testing the preliminary observation of an approximately 90° rotation in S_{Hmax} between the younger and older portions of the Pacific plate and to constrain the magnitudes of

stresses acting on this, the fastest moving, plate.

Second, to understand fully the origins of lithospheric stresses, we must constrain both stress orientations and magnitudes. Hydraulic-fracturing stress-magnitude measurements in a limited number of deep holes (in both the continents and oceans) are clearly needed to understand the stress-boundary conditions on the plates as well as to constrain the stress levels required for intraplate deformation.

Once information on both stress orientation and magnitude becomes available, detailed modelling will be possible of the various sources of stress acting on different plates. Such models, when sufficiently constrained by data, should lead to a greatly improved understanding of plate-tectonic processes. □

1. Hast, N. *Tectonophysics* **8**, 169–211 (1969).
2. Sbar, M. L. & Sykes, L. R. *Bull. geol. Soc. Am.* **84**, 1861–1882 (1973).
3. Sykes, L. R. *Geodynamics of Iceland and the North Atlantic* 207–224 (Reidel, Dordrecht, 1974).
4. Ahorner, L. *Tectonophysics* **29**, 233–249 (1975).
5. Hainson, B. C. *Geophys. Monog. Ser.* **20**, 575–592 (American Geophysical Union, 1977).
6. Sbar, M. L. & Sykes, L. R. *J. geophys. Res.* **82**, 5571–5786 (1977).
7. Greiner, G. & Illies, J. H. *Pure appl. Geophys.* **115**, 11–26 (1977).
8. Illies, J. H. & Greiner, G. *Bull. geol. Soc. Am.* **89**, 770–782 (1978).
9. Illies, J. H. & Greiner, G. *Tectonophysics* **52**, 349–359 (1979).
10. Schmitt, T. J. *Allgemeine Vermessungs-Nachrichten* **86**, 367–370 (1979).
11. Zoback, M. L. & Zoback, M. D. *J. geophys. Res.* **85**, 6113–6156 (1980).
12. Forsyth, D. W. & Uyeda, S. *Geophys. J. R. astr. Soc.* **43**, 163–200 (1975).
13. Chapple, W. M. & Tullis, T. E. *J. geophys. Res.* **82**, 1967–1984 (1977).
14. Harper, J. F. *Geophys. J. R. astr. Soc.* **40**, 465–474 (1975).
15. Harper, J. F. *Geophys. J. R. astr. Soc.* **55**, 87–110 (1978).
16. Harper, J. F. *Geophys. J. R. astr. Soc.* **87**, 155–171 (1986).
17. Bott, M. H. P. *The Interior of the Earth: Its Structure, Constitution, and Evolution* 403 (Edward Arnold, London, 1982).
18. Bott, M. H. P. & Kusnir, N. J. *Tectonophysics* **105**, 1–13 (1984).
19. Richardson, R. M., Solomon, S. C. & Sleep, N. H. *Rev. Geophys. Space Phys.* **17**, 981–1019 (1979).
20. Lachenbruch, A. H. & Sass, J. H. *J. geophys. Res.* **85**, 6185–6222 (1980).
21. Turcotte, D. L. *Geophys. J. R. astr. Soc.* **36**, 33–42 (1974).
22. Artyushkov, E. V. *J. geophys. Res.* **78**, 7675–7708 (1973).
23. Fleitout, L. & Froidevaux, C. *Tectonics* **1**, 21–56 (1982).
24. Mount, V. & Suppe, J. *Geology* **15**, 1143–1147 (1987).
25. Zoback, M. D. *et al. Science* **238**, 1105–1111 (1987).
26. Walcott, R. I. *Geophys. J. R. astr. Soc.* **52**, 137–164 (1978).
27. Anderson, E. M. *The Dynamics of Faulting and Dyke Formation with Applications to Britain* 206 (Oliver and Boyd, Edinburgh, 1951).
28. Zoback, M. L. & Zoback, M. D. *Mem. geol. Soc. Am.* (in the press).
29. Kirsch, G. *Zeitschrift des Vereines Deutscher Ingenieure* **42**, 707–807 (1898), derivation given in Timoshenko, S. & Goodier, J. N. *Theory of Elasticity*, 2nd edition (McGraw-Hill, New York, 1951).
30. Gough, D. I. & Bell, J. S. *Can. J. Earth Sci.* **18**, 638–645 (1981).
31. Zoback, M. D., Moos, D., Mastin, L. & Anderson, R. N. *J. geophys. Res.* **90**, 5523–5530 (1985).
32. Hickman, S. H., Healy, J. H. & Zoback, M. D. *J. geophys. Res.* **90**, 5497–5512 (1985).
33. Shamir, G., Zoback, M. D. & Barton, C. A. *Geophys. Res. Lett.* **15**, 989–992 (1988).
34. Stock, J. M., Healy, J. H., Hickman, S. H. & Zoback, M. D. *J. geophys. Res.* **90**, 8691–8706 (1986).
35. Lacy, L. *Soc. Petrol. Engng. 59th A. Fall Tech. Conf.* (1984).
36. Bell, J. S. & Gough, D. I. *Earth planet. Sci. Lett.* **45**, 475–482 (1979).
37. Gough, D. I. & Bell, J. S. *Can. J. Earth Sci.* **19**, 1958–1970 (1982).
38. Suter, M. J. *J. geophys. Res.* **92**, 2617–2626 (1987).
39. Plumb, R. & Cox, J. J. *J. geophys. Res.* **92**, 4805–4816 (1987).
40. Dzeiwonski, A. M. & Woodhouse, J. H. *J. geophys. Res.* **88**, 3247–3272 (1983).
41. McKenzie, D. P. *Bull. Seismol. Soc. Am.* **59**, 591–601 (1969).
42. Raleigh, C. B., Healy, J. H. & Bredehoeft, J. D. *Geophys. Monogr. Ser.* **16**, 275–284 (1972).
43. Sibson, R. H. *Nature* **249**, 542–543 (1974).
44. Wallace, R. E. *J. Geol.* **59**, 118–130 (1951).
45. Bott, M. H. P. *Geol. Mag.* **96**, 109–117 (1959).
46. Angelier, J. *Tectonophysics* **56**, 17–26 (1979).
47. Vasseur, G., Etchecopar, A. & Philip, H. *Annales Geophysicae* **1**, 291–298 (1983).
48. Angelier, J. *J. geophys. Res.* **89**, 5835–5848 (1984).
49. Gephart, J. W. & Forsyth, D. W. *J. geophys. Res.* **89**, 9305–9320 (1984).
50. Michael, A. J. *J. geophys. Res.* **92**, 357–368 (1987).
51. Carey-Gailhardis, E. & Mercier, J. L. *Earth planet. Sci. Lett.* **82**, 165–179 (1987).
52. Sbar, M. L. *Geophys. Res. Lett.* **10**, 177–180 (1982).
53. King, G. C. P. *Pageoph* **121**, 761–815 (1983).
54. Deschamps, A. & King, G. C. P. *Earth planet. Sci. Lett.* **62**, 296–304 (1983).
55. Oppenheimer, D. H., Reasenberg, P. A. & Simpson, R. W. *J. geophys. Res.* **93**, 9007–9026 (1988).
56. Mercier, J. L. & Carey-Gailhardis, E. *Earth planet. Sci. Lett.* **92**, 247–264 (1989).
57. Carey, E. *Rev. geol. Dyn. geogr. Phys.* **21**, 57–66 (1979).
58. Michael, A. J. *J. geophys. Res.* **89**, 11517–11526 (1984).
59. Reches, Z. *Tectonics* **6**, 849–861 (1987).
60. Nakamura, K. *J. volcanol. geotherm. Res.* **2**, 1–16 (1977).
61. Anderson, E. M. *Proc. R. Soc. Edinb. Ser. B* **58**, 242–251 (1938).
62. McGarr, A. & Gay, N. C. A. *Rev. Earth planet. Sci.* **6**, 405–436 (1978).
63. Engelder, T. & Sbar, M. J. *geophys. Res.* **89**, 9321–9322 (1984).
64. Ranalli, G. & Chandler, T. E. *Geol. Rundschau* **64**, 653–674 (1975).
65. Minster, J. B. & Jordan, T. H. *J. geophys. Res.* **83**, 5331–5354 (1978).
66. Dart, R. L. & Zoback, M. L. *US Open File Rep.* **87-283**, 43 (1987).
67. Gough, D. I., Fordjor, C. K. & Bell, J. S. *Nature* **305**, 619–621 (1983).
68. Zoback, M. L. *et al. The Geology of North America, Volume M, The Western North Atlantic Region* 297–312 (Geological Society of America, 1986).
69. Hasegawa, H. S., Adams, J. & Yamazaki, K. *J. geophys. Res.* **90**, 3637–3648 (1985).
70. Richardson, R. M. & Reding, L. M. *J. geophys. Res.* (in the press).
71. Brereton, N. R. & Evans, C. J. *Rep. Regional Geophys. Res. Group RG/87/14* 98 (British Geological Survey, 1987).
72. DeMets, C., Gordon, R. G., Argus, D. F. & Stein, S. *Geophys. J. Int.* (in the press).
73. Parsons, B. & Sclater, J. G. *J. geophys. Res.* **82**, 803–827 (1977).
74. Molnar, P. & Tapponnier, P. *Science* **189**, 419–426 (1975).
75. Cloetingh, S. & Wortel, R. *Geophys. Res. Lett.* **12**, 77–80 (1985).
76. Cloetingh, S. & Wortel, R. *Tectonophysics* **132**, 49–67 (1986).
77. Wiens, D. A., Stein, S., DeMets, C., Gordon, R. G. & Stein, C. *Tectonophysics* **132**, 37–48 (1986).
78. Mercier, J. L., Sorel, D. & Simeakis, K. *Annales Tectonicae* **1**, 20–39 (1987).
79. England, P. & Houseman, G. A. *J. geophys. Res.* (in the press).
80. Braile, L. W., Hinze, W. J., von Frese, R. R. B. & Keller, G. R. *Mem. geol. Soc. Am.* (in the press).
81. Zoback, M. L. *J. geophys. Res.* **94**, 7105–7128 (1989).
82. McGarr, A. J. *geophys. Res.* **87**, 9279–9288 (1982).
83. Shudofsky, G. N. *Geophys. J. R. astr. Soc.* **83**, 563–614 (1985).
84. Newmark, R., Zoback, M. D. & Anderson, R. N. *Nature* **311**, 424–428 (1984).

ACKNOWLEDGEMENTS. In addition to the authors, all of whom have compiled data for the project, the following individuals are currently working on data sets to be contributed: D. Fairhead, University of Leeds, UK; T. N. Gowd, National Geophysical Research Institute, India; N. Pavoni, Institut für Geophysics, ETH, Switzerland; Z. Reches, Hebrew University, Israel; and M. Untung, Indonesia. We gratefully acknowledge reviews by R. W. Simpson and A. McGarr. The US Nuclear Regulatory Commission has provided funding for much of the breakout analysis in the United States done by M.L.Z.